C. Tantos, G.P. Ghiroldi, D. Valougeorgis, A. Frezzotti
Effect of Vibrational Degrees of Freedom on the Heat Transfer in Polyatomic Gases Confined Between Parallel Plates
International Journal of Heat and Mass Transfer, Vol. 102, 2016, p. 162-173
doi:10.1016/j.ijheatmasstransfer.2016.06.010

Effect of vibrational degrees of freedom on the heat transfer in polyatomic gases confined between parallel plates

Christos Tantos[1], Gian Pietro Ghiroldi[2], Dimitris Valougeorgis[1*], Aldo Frezzotti[2]

[1]Department of Mechanical Engineering, University of Thessaly
Pedion Areos, 38334 Volos, Greece

[2]Dipartimento di Scienze & Tecnologie Aerospaziali, Politecnico di Milano
Via La Masa 34, 20156 Milano, Italy

Keywords: Kinetic theory, Polyatomic gases, Vibrational modes, Holway model, DSMC, Sulfur hexafluoride, Micro heat transfer.

Abstract

Conductive stationary heat transfer through rarefied nonpolar polyatomic gases, confined between parallel plates maintained at different temperatures, is investigated. It is assumed that gas molecules possess both rotational and vibrational degrees of freedom, described by the classical rigid rotator and quantum harmonic oscillator models, respectively. The flow structure is computed by the Holway kinetic model and the Direct Simulation Monte Carlo method. In both approaches the total collision frequency is computed according to the Inverse Power Law intermolecular potential. Anelastic collisions in DSMC simulations are based on the quantum version of the Borgnakke-Larsen collision model. Results are presented for N_2, O_2, CO_2, CH_4 and SF_6 representing diatomic as well as linear and nonlinear polyatomic molecules with 1 up to 15 vibrational modes. The translational, rotational, vibrational and total temperatures and heat fluxes are computed in a wide range of the rarefaction parameter and for various ratios of the hot over the cold plate temperatures. Very good agreement, between the Holway and DSMC results is observed as well as with experiments. The effect of the vibrational degrees of freedom is demonstrated. In diatomic gases the vibrational heat flux varies from 5% up to 25% of the total one. Corresponding results in polyatomic gases with a higher number of vibrational modes show that even at low reference temperatures the contribution of the vibrational heat flux may be considerably higher. For example in the case of SF_6 at 300 K and 500 K the vibrational heat flux is about 67% and 76% respectively of the total heat flux. Furthermore, it is numerically proved that the computed solutions are in agreement with the Chapman-Enskog approximation in a central strip of the computational domain even at moderately large values of the rarefaction parameter, as found in previous investigations. This property has been used to compute the gas thermal conductivity predicted by the adopted models.

---

*Corresponding author: diva@mie.uth.gr

1. Introduction

Heat transfer through stationary rarefied monatomic gases confined between solid boundaries has attracted over the years considerable attention. The literature survey on this topic is very extensive and therefore only some indicative works related to the present heat transfer configuration are cited [1-6]. Corresponding work in polyatomic gases is quite limited and the existing one ignores the effect of the vibrational degrees of freedom [7-14]. It is known however, that vibrational excitation must be included when the reference temperature of the heat flow setup exceeds about 30% of the lower gas characteristic vibrational temperature which significantly varies for each gas. For instance, for N_2 and O_2 it is $3371\,\mathrm{K}$ and $2256\,\mathrm{K}$ respectively, whereas for CO_2 is $960\,\mathrm{K}$ and for SF_6 is $520\,\mathrm{K}$.

Polyatomic gases with relatively low and moderate characteristic vibrational temperatures are very common in several industrial processes and technological applications running in a wide range of operating temperatures. A typical example of low excitation temperature gases is SF_6, which is used in power plants (gas insulator switchgears and circuit breakers), in the electronics industry (plasma etching and chemical vapor deposition), in the magnesium production (die casting) and in other applications including gas-air tracing, leak detection, soundproof windows, etc. [15-17]. Other gases with moderate excitation temperatures may be involved in piezoelectric sensing technologies [18,19] at high temperatures ($>800\,^{o}\mathrm{C}$) in the automotive industry and in micro-electro-mechanical systems for aeronautics and space applications (e.g. micro rocket engines) [20], as well as in natural and environmental processes. Modeling of these processes should include the effect of the excited vibrational modes, if agreement between measurements and calculations is to be obtained.

Having all these considerations in mind, it is interesting and useful to investigate in a complete and precise manner the contribution of the vibrational degrees of freedom in a simple problem of heat transfer through polyatomic gases in a wide range of reference temperatures and gas rarefaction. It is also important to examine the effect of the various characteristic vibrational temperatures and corresponding number of vibrational degrees of freedom on the computed macroscopic quantities.

In the present work, the stationary heat transfer flow through rarefied nonpolar polyatomic gases, confined between two parallel plates, is simulated both deterministically and

stochastically by implementing the Holway kinetic model and the DSMC scheme respectively for gases whose molecules possess both rotational and vibrational degrees of freedom. The translational, rotational, vibrational and total temperature and heat flux distributions are presented for a wide range of the involved parameters. Comparisons between the kinetic model and the DSMC method as well as between simulations and experimental data [21] are shown and discussed. The influence of the vibrational degrees of freedom on the heat fluxes for CO_2, CH_4 and SF_6 at low reference temperatures is investigated, while corresponding high temperature calculations with N_2 and O_2 is mainly performed for model testing and results validation. Furthermore, thermal conductivities predicted by the considered gas models have been estimated exploiting the good agreement between the kinetic solutions and their hydrodynamic (Chapman-Enskog) approximations, which occurs, even for moderately high values of the rarefaction parameter in a central strip of the domain [22,23,24].

2. Heat transfer configuration and basic definitions

Consider the state of a stationary nonpolar polyatomic gas confined between two infinite parallel plates fixed at $\hat{y} = \pm H/2$ and maintained at constant temperatures T_H and T_C respectively, with $T_H > T_C$. Then, due to temperature difference a conductive heat flow through the gas from the hot to the cold plate is induced.

The adopted models include translational, rotational and vibrational energy modes of the molecules assuming that the translational and the rotational energies are continuous, while the vibrational energy is discrete. The rotation and vibration of the gas molecules are described by the rigid rotator and the quantum harmonic oscillator models respectively. The rotational mode can be described as having a constant number of degrees of freedom at all temperatures which is $j = 2$ for linear molecules and $j = 3$ for non-linear molecules.

On the contrary, the effective number of vibrational degrees of freedom varies with temperature. For the simple quantum harmonic oscillator assumed here they are defined as [25]

$$\zeta_v(T) = \frac{2}{T}\sum_{i=1}^{N}\frac{\Theta_{V,i}}{\exp\left[\Theta_{V,i}/T\right]-1}, \qquad (1)$$

where N is the total number of vibrational modes given by $N = 3M - 5$ for linear molecules and $N = 3M - 6$ for nonlinear molecules with M being the number of atoms in the molecule. Also, $\Theta_{V,i}$ is the characteristic vibrational temperature of vibrational mode i given by [25]

$$\Theta_{V,i} = \frac{\hbar \varpi_i}{k_B}, \tag{2}$$

where $\hbar = 1.05457 \times 10^{-34}$ J s is the reduced Planck constant, ϖ_i is the vibrational frequency of the gas molecules and $k_{\mathrm{B}} = 1.38065 \times 10^{-23}$ J/K is the Boltzmann constant. In diatomic gases at high temperature $\zeta_v \to 2$, while in polyatomic gases ζ_v takes higher values depending on the specific gas and the applied temperature.

In the absence of dissociation, the state of a polyatomic gas is determined by its distribution function $\hat{f}_S\left(\hat{y}, \boldsymbol{v}, \hat{I}\right)$, where $S = \{S_1, S_2, \ldots S_N\}$, with $S_i = 0, 1, 2, \ldots$, represents the vibrational quantum states, that depends on the space coordinate $\hat{y}$, the molecular translational velocity $\boldsymbol{v} = \left(\xi_x, \xi_y, \xi_z\right)$ and the energy of rotational motion $\hat{I}$ [25,26]. Then, the macroscopic quantities of practical interest are obtained by the moments of $\hat{f}_S$ as [26,27]

$$n(\hat{y}) = \sum_{S=0}^{\infty} \int_{-\infty}^{\infty} \int_{0}^{\infty} \hat{f}_S d\hat{I} d\boldsymbol{v}, \tag{3}$$

$$E_{tr}(\hat{y}) = \frac{3k_B T_{tr}(\hat{y})}{2} = \frac{m}{2n} \sum_{S=0}^{\infty} \int_{-\infty}^{\infty} \int_{0}^{\infty} v^2 \hat{f}_S d\hat{I} d\boldsymbol{v}, \tag{4}$$

$$E_{rot}(\hat{y}) = \frac{jk_B T_{rot}(\hat{y})}{2} = \frac{1}{n} \sum_{S=0}^{\infty} \int_{-\infty}^{\infty} \int_{0}^{\infty} \hat{I} \hat{f}_S d\hat{I} d\boldsymbol{v}, \tag{5}$$

$$E_{vib}(\hat{y}) = \frac{\zeta_v\left(T_{vib}(\hat{y})\right) k_B T_{vib}(\hat{y})}{2} = \frac{1}{n} \sum_{S=0}^{\infty} \int_{-\infty}^{\infty} \int_{0}^{\infty} \left(\sum_{i=1}^{N} \hbar \varpi_i S_i \right) \hat{f}_S d\hat{I} d\boldsymbol{v}, \tag{6}$$

$$Q_{tr}(\hat{y}) = \frac{m}{2} \sum_{S=0}^{\infty} \int_{-\infty}^{\infty} \int_{0}^{\infty} \xi_{\hat{y}} v^2 \hat{f}_S d\hat{I} d\boldsymbol{v}, \tag{7}$$

$$Q_{rot}(\hat{y}) = \sum_{S=0}^{\infty} \int_{-\infty}^{\infty} \int_{0}^{\infty} \xi_{\hat{y}} \hat{I} \hat{f}_S d\hat{I} d\boldsymbol{v}, \tag{8}$$

$$Q_{vib}\left(\hat{y}\right)=\sum_{S=0}^{\infty}\int_{-\infty}^{\infty}\int_{0}^{\infty}\xi_{\hat{y}}\left(\sum_{i=1}^{N}\hbar\varpi_i S_i\right)\hat{f}_S d\hat{I}d\boldsymbol{\upsilon}\,, \tag{9}$$

$$T_{tot}\left(\hat{y}\right)=\frac{3\,T_{tr}\left(\hat{y}\right)+j\,T_{rot}\left(\hat{y}\right)+\zeta_v\left(T_{vib}\left(\hat{y}\right)\right)T_{vib}\left(\hat{y}\right)}{3+j+\zeta_v\left(T_{tot}\left(\hat{y}\right)\right)}, \tag{10}$$

$$Q_{tot}\left(\hat{y}\right)=Q_{tr}\left(\hat{y}\right)+Q_{rot}\left(\hat{y}\right)+Q_{vib}\left(\hat{y}\right), \tag{11}$$

In Eqs. (3-11), $n\left(\hat{y}\right)$ is the number density, $E_{tr}\left(\hat{y}\right)$, $E_{rot}\left(\hat{y}\right)$, $E_{vib}\left(\hat{y}\right)$ are the mean particle energies and $Q_{tr}\left(\hat{y}\right)$, $Q_{rot}\left(\hat{y}\right)$, $Q_{vib}\left(\hat{y}\right)$ are the heat fluxes related to the translational, rotational and vibrational motion of the molecules respectively, with $T_{tr}\left(\hat{y}\right)$, $T_{rot}\left(\hat{y}\right)$, $T_{vib}\left(\hat{y}\right)$ denoting the corresponding temperatures. Also $T_{tot}\left(\hat{y}\right)$ is the total temperature and $Q_{tot}\left(\hat{y}\right)$ is the total heat flux of all degrees of freedom.

The problem in dimensionless form is prescribed by the ratio of the high over the low plate temperatures

$$\beta=T_H/T_C \tag{12}$$

and the reference gas rarefaction parameter

$$\delta_0=\frac{P_0 H}{\mu_0\upsilon_0}, \tag{13}$$

where μ_0 is the gas viscosity at reference temperature $T_0=\left(T_H+T_C\right)/2$, $P_0=n_0k_BT_0$ is the reference pressure and $\upsilon_0=\sqrt{2k_{\mathrm{B}}T_0/m}$, with m denoting the molecular mass, is the most probable molecular speed at T_0. The cases of $\delta_0=0$ and $\delta_0\to\infty$ correspond to the free molecular and hydrodynamic limits respectively. In addition, the dimensionless vibrational temperatures

$$\theta_{V,i}=\Theta_{V,i}/T_0\,, \tag{14}$$

depending upon the working gas under consideration, are specified.

Furthermore, it is convenient to introduce the following dimensionless variables and macroscopic quantities:

$$y=\hat{y}/H\,,\quad \boldsymbol{c}=\boldsymbol{\upsilon}/\upsilon_0\,,\quad I=\hat{I}/\left(k_{\mathrm{B}}T_0\right),\quad f_S=\hat{f}_S\upsilon_0^3k_{\mathrm{B}}T_0/n_0\,,\quad \rho=n/n_0\,,\quad \tau_i=T_i/T_0\,,$$

$$q_i=Q_i/\left(P_0\upsilon_0\right),\quad e_i=E_i/\left(k_{\mathrm{B}}T_0\right) \tag{15}$$

In the above expressions $n_0 = \frac{1}{H}\int_{-H/2}^{H/2} n(\hat{y})\,d\hat{y}$ is a reference number density and the subscript $i = tr, rot, vib, tot$ refers to translational, rotational, vibrational or total quantities. The effect of all involved parameters on the heat transfer problem is investigated focusing on the effect of $\theta_{V,i}$ since it is the parameter which characterizes the importance of the vibrational degrees of freedom. This is achieved via the Holway kinetic model and the DSMC method described in Sections 3 and 4 respectively.

3. The Holway kinetic model

The Boltzmann equation is the fundamental equation describing the motion of gas molecules from the continuum-fluid to the free-molecular flow regimes. However, its collision operator makes a solution difficult to be obtained by deterministic numerical methods. The effort of solving the Boltzmann equation is significantly reduced by substituting the complicated collision term with reliable kinetic models.

The Holway kinetic model [26] has been applied with considerable success in rarefied polyatomic gas flows and heat transfer configurations [27,10,12,14] providing good agreement with experimental results. The H-theorem can be proved in a straightforward manner for the Holway model following the arguments leading to analogous proof for the BGK model [12,14]. The Holway model in its applied form does not recover both the shear viscosity and thermal conductivity simultaneously and since here a purely heat transfer configuration is investigated the collision frequency has been set to properly recover the thermal conductivity coefficient.

The Holway model for the present heat transfer configuration can be written as

$$\xi_y \frac{\partial \hat{f}_S}{\partial \hat{y}} = \hat{\nu}_{tot}\left[\left(1-\frac{1}{Z_{rot}^{(H)}}-\frac{1}{Z_{vib}^{(H)}}\right)\left(\hat{f}_S^{(tr)}-\hat{f}_S\right)+\frac{1}{Z_{rot}^{(H)}}\left(\hat{f}_S^{(tr,rot)}-\hat{f}_S\right)+\frac{1}{Z_{vib}^{(H)}}\left(\hat{f}_S^{(tr,rot,vib)}-\hat{f}_S\right)\right], \qquad (16)$$

where

$$\hat{f}_S^{(tr)} = n_S(\hat{I}\,|\,\hat{y})\left(\frac{m}{2\pi k_B T_{tr}}\right)^{3/2}\exp\left(-\frac{m\upsilon^2}{2k_B T_{tr}}\right), \qquad (17)$$

$$\hat{f}_S^{(tr,rot)} = \hat{n}_S(\hat{y})\left(\frac{m}{2\pi k_B T^r}\right)^{3/2}\exp\left(-\frac{m\upsilon^2}{2k_B T^r}\right)\frac{\hat{I}^{j/2-1}}{\Gamma(j/2)\left(k_B T^r\right)^{j/2}}\exp\left(-\frac{\hat{I}}{k_B T^r}\right), \qquad (18)$$

$$\hat{f}_S^{(tr,rot,vib)} = n\left(\frac{m}{2\pi k_{\mathrm{B}} T_{tot}}\right)^{3/2} \exp\left(-\frac{\frac{m\,v^2}{2}+\sum_{i=1}^{N}\hbar\varpi_i S_i+\hat{I}}{k_{\mathrm{B}}T_{tot}}\right)\frac{\hat{I}^{\,j/2-1}}{\Gamma\left(j/2\right)\left(k_{\mathrm{B}}T_{tot}\right)^{j/2}}\prod_{i=1}^{N}\left[1-\exp\left(-\frac{\hbar\varpi_i}{k_{\mathrm{B}}T_{tot}}\right)\right]. \quad (19)$$

Here, $\hat{\nu}_{tot} = \left[\Pr\left(T_{tr}\right) n k_{\mathrm{B}} T_{tr}\right] \big/ \mu\left(T_{tr}\right)$ is the total collision frequency where $\Pr\left(T_{tr}\right)$ is the Prandtl number and $\mu\left(T_{tr}\right)$ is the viscosity both depending on the translational temperature. The parameters $1 \le Z_{rot}^{(H)},\ Z_{vib}^{(H)} < \infty$ define respectively the number of rotational and vibrational collisions per one elastic collision. It is noted that $Z_{rot}^{(H)},\ Z_{vib}^{(H)}$ must be chosen in such a way that the rotational and vibrational relaxations governed by the Holway model match the corresponding relaxations obtained by the DSMC method when these approaches are compared. This task is performed in Appendix A. Also n is the total number density defined by Eq. (3), $\hat{n}_S$ is the total number density in vibrational state S and n_S is the number density of molecules having rotational energy $\hat{I}$ in vibrational state S. Finally, $T^r\left(\hat{y}\right)$ is the common temperature of the rotational and translational modes given by $T^r\left(\hat{y}\right) = \left[3T_{tr}\left(\hat{y}\right) + jT_{rot}\left(\hat{y}\right)\right] \big/ \left(3+j\right)$.

In order to reduce the computational cost the following three reduced density distributions one for the mass and two for the internal energy (rotational and vibrational) are introduced [28,10,29]

$$\hat{G} = \sum_{S=0}^{\infty}\int_0^{\infty} \hat{f}_S d\hat{I}, \qquad \hat{R} = \sum_{S=0}^{\infty}\int_0^{\infty} \hat{I}\,\hat{f}_S d\hat{I}, \qquad \hat{V} = \sum_{s=0}^{\infty}\int_0^{\infty}\left(\sum_{i=1}^{N}\hbar\varpi_i S_i\right)\hat{f}_S d\hat{I}. \quad (20)$$

For the specific problem under consideration the computational effort is further reduced by eliminating the ξ_x and ξ_z components of the molecular velocity by introducing the reduced distributions

$$\hat{F} = \int_{-\infty}^{\infty}\int_{-\infty}^{\infty} \hat{G}\, d\xi_x d\xi_z,\ \ \hat{L} = \int_{-\infty}^{\infty}\int_{-\infty}^{\infty} \hat{G}\left(\xi_z^2+\xi_x^2\right) d\xi_x d\xi_z,\ \ \hat{H} = \int_{-\infty}^{\infty}\int_{-\infty}^{\infty} \hat{R}\, d\xi_x d\xi_z,\ \ \hat{K} = \int_{-\infty}^{\infty}\int_{-\infty}^{\infty} \hat{V}\, d\xi_x d\xi_z. \quad (21)$$

Operating accordingly with the appropriate summation and integral operators, defined by expressions (20) and (21), on Eqs. (16) and introducing the dimensionless quantities of Eq. (15)

along with the dimensionless reduced distributions $F=\upsilon_0\hat{F}/n_0$, $L=\hat{L}/(n_0\upsilon_0)$, $H=\upsilon_0\hat{H}/P_0$ and $K=\upsilon_0\hat{K}/P_0$ the following system of kinetic equations may be obtained in vector form:

$$c_y\frac{\partial\boldsymbol{\Psi}}{\partial y}=\nu_{tot}\left[\left(1-\frac{1}{Z_{rot}^{(H)}}-\frac{1}{Z_{vib}^{(H)}}\right)\left(\boldsymbol{\Psi}^{(tr)}-\boldsymbol{\Psi}\right)+\frac{1}{Z_{rot}^{(H)}}\left(\boldsymbol{\Psi}^{(tr,rot)}-\boldsymbol{\Psi}\right)+\frac{1}{Z_{vib}^{(H)}}\left(\boldsymbol{\Psi}^{(tr,rot,vib)}-\boldsymbol{\Psi}\right)\right] \qquad (22)$$

Here, $\boldsymbol{\Psi}=\left[F,L,H,K\right]^T$ are the unknown reduced distributions, which depend on the dimensionless independent variables of space y and molecular velocity c_y . Also, $\nu_{tot}=\delta_0\rho\left(\tau_{tr}\right)^{1-\omega}\Pr\left(\tau_{tr}\right)$ is the dimensionless collision frequency and δ_0 is the reference gas rarefaction given by Eq. (13). The relaxing distributions in Eq. (22) are given by $\boldsymbol{\Psi}^{(i)}=\left[F^{(i)},L^{(i)},H^{(i)},K^{(i)}\right]^T$, with $i=(tr),(tr,rot),(tr,rot,vib)$, where

$$F^{(tr)}=\frac{\rho}{\sqrt{\pi\tau_{tr}}}\exp\left(-\frac{c_y^2}{\tau_{tr}}\right),\quad F^{(tr,rot)}=\frac{\rho}{\sqrt{\pi\tau^r}}\exp\left(-\frac{c_y^2}{\tau^r}\right),\quad F^{(tr,rot,vib)}=\frac{\rho}{\sqrt{\pi\tau_{tot}}}\exp\left(-\frac{c_y^2}{\tau_{tot}}\right),$$

$$L^{(tr)}=\tau_{tr}F^{(tr)},\quad L^{(tr,rot)}=\tau^rF^{(tr,rot)},\quad L^{(tr,rot,vib)}=\tau_{tot}F^{(tr,rot,vib)},$$

$$H^{(tr)}=\frac{j}{2}\tau_{rot}F^{(tr)},\quad H^{(tr,rot)}=\frac{j}{2}\tau^rF^{(tr,rot)},\quad H^{(tr,rot,vib)}=\frac{j}{2}\tau_{tot}F^{(tr,rot,vib)},$$

$$K^{(tr)}=\frac{\zeta_v\left(\tau_{vib}\right)}{2}\tau_{vib}F^{(tr)},\ K^{(tr,rot)}=\frac{\zeta_v\left(\tau_{vib}\right)}{2}\tau_{vib}F^{(tr,rot)},\ K^{(tr,rot,vib)}=\frac{\zeta_v\left(\tau_{tot}\right)}{2}\tau_{tot}F^{(tr,rot,vib)}. \qquad (23)$$

In the derivation of Eq. (22) the Inverse Power Law (IPL) interaction [29] between particles has been introduced with the parameter ω taking the values of $1/2$ and 1 for hard sphere (HS) and Maxwell (MM) interactions respectively.

The same non-dimensionalization and projection procedures are applied to the moments (3-11), to find that the macroscopic quantities are given in terms of F , L , H and K according to

$$\rho=\int_{-\infty}^{\infty}F dc_y\ ,\quad q_{tr}=\int_{-\infty}^{\infty}\left(c_y^2F+L\right)c_y dc_y\ ,\quad q_{rot}=\int_{-\infty}^{\infty}Hc_y dc_y\ ,\quad q_{vib}=\int_{-\infty}^{\infty}Kc_y dc_y\ ,\ q_{tot}=q_{vib}+q_{rot}+q_{tr}$$

$$e_{tr}=\frac{3\tau_{tr}}{2}=\frac{1}{\rho}\int_{-\infty}^{\infty}\left(c_y^2F+L\right)dc_y\ ,\quad e_{rot}=\frac{j\tau_{rot}}{2}=\frac{1}{\rho}\int_{-\infty}^{\infty}Hdc_y\ ,\quad e_{vib}=\frac{\zeta_v\left(\tau_{vib}\right)\tau_{vib}}{2}=\frac{1}{\rho}\int_{-\infty}^{\infty}Kdc_y\ ,$$

$$\tau^r = \frac{3\,\tau_{tr} + j\,\tau_{rot}}{3+j}, \qquad \tau_{tot} = \frac{3\,\tau_{tr} + j\,\tau_{rot} + \zeta_v\left(\tau_{vib}\right)\tau_{vib}}{3+j+\zeta_v\left(\tau_{tot}\right)}, \tag{24}$$

where

$$\zeta_v\left(\tau_{vib}\right) = \frac{2}{\tau_{vib}}\sum_{i=1}^{N}\theta_{V.i}\Bigg/\left[\exp\left(\frac{\theta_{V.i}}{\tau_{vib}}\right)-1\right] \quad \text{and} \quad \zeta_v\left(\tau_{tot}\right) = \frac{2}{\tau_{tot}}\sum_{i=1}^{N}\theta_{V.i}\Bigg/\left[\exp\left(\frac{\theta_{V.i}}{\tau_{tot}}\right)-1\right] \tag{25}$$

are the vibrational degrees of freedom in dimensionless temperatures τ_{vib} and τ_{tot} respectively. From Eq. (22) the energy conservation equation $\partial q_{tot}/\partial y = 0$ is readily reduced and it is implemented to benchmark the computations.

Next, the boundary conditions are defined. The typical purely diffuse boundary conditions are implemented where the distribution function of the particles departing by the two plates takes the form [26]

$$f_S^{(+)} = n_w\left(\frac{m}{2\pi k_{\mathrm{B}}T_w}\right)^{3/2}\frac{\hat{I}^{\,j/2-1}}{\Gamma\left(j/2\right)\left(k_{\mathrm{B}}T_w\right)^{j/2}}\exp\left(-\frac{\frac{m\,v^2}{2}+\hat{I}+\sum_{i=1}^{N}\hbar\varpi_i S_i}{k_{\mathrm{B}}T_w}\right)\prod_{i=1}^{N}\left[1-\exp\left(-\frac{\hbar\varpi_i}{k_{\mathrm{B}}T_w}\right)\right]. \tag{26}$$

The superscript $(+)$ denotes outgoing distributions, $T_w\left(\pm 1/2\right)$ is either the cold or the hot temperatures of the plates and $n_w\left(\pm 1/2\right)$ is a parameter specified by the condition of no penetration at the walls. Introducing in Eq. (26), the same normalization and projection as for the kinetic equations, lead to the outgoing distributions

$$F_{\pm 1/2}^{(+)} = \frac{\rho_{w,\pm 1/2}}{\sqrt{\pi\tau_w}}\exp\left(-\frac{c_y^2}{\tau_w}\right),\; L_{\pm 1/2}^{(+)} = \tau_w F_{\pm 1/2}^{(+)},\; H_{\pm 1/2}^{(+)} = \frac{j}{2}\tau_w F_{\pm 1/2}^{(+)},\; K_{\pm 1/2}^{(+)} = \frac{\tau_w\zeta_v\left(\tau_w\right)}{2}F_{\pm 1/2}^{(+)}, \tag{27}$$

at $y = \pm 1/2$, where ρ_w is specified by applying the no penetration condition at the walls as

$$\rho_{w,\pm 1/2} = \frac{2\sqrt{\pi}}{\sqrt{\tau_w}}\int_0^{\infty} F_{\pm 1/2}^{(-)} c_y dc_y\,. \tag{28}$$

In Eqs. (27) and (28) the superscripts $(+)$ and $(-)$ denote outgoing and impinging distributions respectively. Also, $\tau_w = T_w/T_0$ and in terms of the temperature ratio β is equal to $2\beta/\left(\beta+1\right)$ at $y = -1/2$ (hot wall) and $2/\left(\beta+1\right)$ at $y = 1/2$ (cold wall).

The governing equations (22-23) with the associated expressions (24) subject to boundary conditions (27-28) are solved numerically in an iterative manner. More specifically for prescribed values of β, δ_0 and $\theta_{V,i}$ the iteration map starts by assuming all needed macroscopic quantities. The kinetic equations (22-23) are solved numerically discretizing in the physical space by the control volume approach and in the molecular velocity space by the discrete velocity method to yield the reduced distributions F, L, H and K, which are introduced into the moment equations (24) and (28). Integration is performed via the Gauss-Legendre quadrature to find the new estimates of all bulk quantities which are introduced in the next iteration. The iteration process is terminated when convergence criteria

$$\frac{1}{3M}\sum_{i=1}^{M}\left[\left|\rho_i^{(t+1)}-\rho_i^{(t)}\right|+\left|\tau_{tot,i}^{(t+1)}-\tau_{tot,i}^{(t)}\right|+\left|q_{tot,i}^{(t+1)}-q_{tot,i}^{(t)}\right|\right]<\varepsilon \tag{29}$$

with t denoting the iteration index and M the number of nodes in the physical space, is fulfilled. The kinetic results presented here have been obtained with $\Delta y = 1/\left(M+1\right) = 0.2\times 10^{-3}$ and 96 molecular velocities being the roots of the corresponding Legendre polynomial.

4. DSMC modeling

A series of DSMC simulations, limited to O_2 and N_2, have been performed, in order to provide additional data to assess the capabilities of the kinetic model. A quite standard setup of DSMC simulations has been used. Total collision cross sections have been computed by VHS model [30], its parameters being tuned on the same viscosity data used to determine the kinetic model collision frequency. Anelastic collisions have been dealt with by Borgnakke-Larsen (BL) model [31] for translational-rotational coupling and by its quantum extension [32] to describe collisions involving vibrational energy transfer. As is well known, BL model describes energy transfer between internal and translational energies by assuming that a fraction of the total number of collisions is *elastic*, i.e. no exchange between internal and translational energy occurs, whereas the remaining fraction is composed by collisions in which rotational and/or vibrational energy is exchanged according to prescribed probabilistic rules. In complete analogy with the kinetic model setup, the probabilities of elastic and anelastic collisions have been assigned through temperature independent values of $Z_{rot}^{(DSMC)}$ and $Z_{vib}^{(DSMC)}$. The same equally spaced vibrational energy levels have been used, according to the quantum linear oscillator model.

However, it should be noted that, although BL model is based on sampling post-collisional states from fictitious equilibrium distributions, its collision frequency depends on the relative velocity of colliding partners, not on translational temperature, as in the case of Holway model. Hence, setting equal values of the rotational and vibrational collision parameters for DSMC and kinetic model does not guarantee identical relaxation rates, which are provided only by developing proper expressions to relate $Z_{rot}^{(H)}$ with $Z_{rot}^{(DSMC)}$ and $Z_{vib}^{(H)}$ with $Z_{vib}^{(DSMC)}$. This procedure along with the derived expressions is outlined in Appendix A.

The numerical setting of each DSMC simulation depended on the particular values of its physical and geometrical parameters. Grid size, time step, particles number and simulation duration have been varied until further refinements led to percentage variations not exceeding 1%. In a typical setting, not less than 10^6 particles have been used. The uniform grid size has been reduced down to 0.025 reference mean free paths whereas the time step has been set equal to $\min\left(0.1\times\tau_{coll}, 0.4\times\tau_{cell}\right)$, being τ_{coll} the smallest mean free time, and τ_{cell} the time a particle takes to cross a cell. Simulation durations extended from 2.5×10^4 to 7.5×10^4 time steps.

5. Results and discussion

Results for the density, temperature and heat flux distributions are obtained by the Holway kinetic model and the DSMC method for $\beta=\left[1.1, 4, 5, 11\right]$ covering small, moderate and large temperature differences, $\delta_0\in\left[0, 100\right]$ representing heat transfer flow from the free molecular up to the slip regime and $\theta_V=\left[0.1, 1, 2, 5\right]$ corresponding to mean temperatures T_0 higher, equal and lower compared to the characteristic vibrational temperature. At $\theta_V=0.1$ almost all vibrational degrees of freedom are fully excited, while at $\theta_V=5$ almost no vibrational excitation occurs.

The results are organized as follows: Benchmarking is displayed in Section 5.1 by comparing the kinetic model with the DSMC results for N_2 and O_2, as well as simulations with experimental data for N_2, CO_2, CH_4 and SF_6. In Section 5.2, general results for all macroscopic quantities are presented for diatomic gases in terms of $\beta, \delta_0, \theta_V$ including a sensitivity analysis of the dependency of the heat fluxes on Z_{rot}, Z_{vib}. Finally, in Section 5.3 results for the specific gases of N_2, O_2, CO_2, CH_4 and SF_6 are presented showing the effect of the vibrational degrees of

freedom on the total heat fluxes and on the translational, rotational and vibrational parts. Following Refs. [22,23,24], effective values of the thermal conductivity are used to estimate its Chapman-Enskog limit. The properties including the characteristic vibrational temperatures of all gases examined in the present work are given in Table 1.

5.1 Benchmarking

The comparison between the Holway kinetic model and the DSMC method is performed considering N_2 and O_2 as working gases ($j = 2$). To have a valid comparison it is ensured that the two approaches have the same relaxation rates and therefore the relaxation parameters of the Holway model are accordingly fixed. Following common practice the DSMC relaxation parameters are set as $Z_{rot}^{(DSMC)} = 5$ and $Z_{vib}^{(DSMC)} = 50$ [25] and then following Appendix A, the Holway relaxation parameters are $Z_{rot}^{(H)} = 2.47$, $Z_{vib}^{(H)} = 24.7$ for N_2 and $Z_{rot}^{(H)} = 2.62$, $Z_{vib}^{(H)} = 26.2$ for O_2. Furthermore, in both approaches the viscosity index takes the values $\omega = 0.74$ for N_2 and $\omega = 0.66$ for O_2 to reproduce the recommended data in [33]. Also, the Pr number in the kinetic model simulations is independent of temperature and equal to $\mathrm{Pr} = 0.764$ and 0.751 for N_2 and O_2 respectively to ensure that the thermal conductivities obtained by the two methods are equal to each other.

In Tables 2 and 3, a comparison between the results obtained by the Holway model and the DSMC method is performed for N_2 and O_2 respectively. In both tables $\delta_0 \in [0, 100]$, $\beta = 5$ and $\theta_V = 1$ (the mean temperature T_0 is taken equal to the characteristic vibrational temperatures of $3371\,\mathrm{K}$ for N_2 and $2256\,\mathrm{K}$ for O_2). In all cases the agreement between the results, taking into account the different models implemented in the two approaches, is very good. The translational heat fluxes computed by the Holway model are smaller than the DSMC ones, while it is the other way around for the rotational and vibrational heat fluxes. The largest relative errors occurs in the vibrational heat fluxes being always however, about $10\,\%$, while in the total heat fluxes is less than $1\,\%$. A similar behavior in the deviation between Holway and DSMC results has been observed even for $\delta_0 > 100$ (not included in Tables 2 and 3). The results at $\delta_0 = 0$ are in excellent agreement with the analytical free molecular ones presented in Appendix B.

The comparison is extended to the number density as well as to the translational, rotational and vibrational temperature distributions plotted in Fig. 1 for various values of values of δ_0. Excellent agreement between the deterministic and stochastic approaches is shown. It is also observed that for large values of δ_0 the translational, rotational and vibrational are thermally equilibrated ($\tau_{tr} = \tau_{rot} = \tau_{vib}$), while as the rarefaction level of the gas is increased the three temperatures depart from each other with the vibrational temperature being higher than the other two.

Next, a comparison with the experimental data in [21] is performed in Fig. 2 based on the Holway kinetic model in terms of the thermal conductivity. More specifically the experimental data for the thermal conductivities of N_2, CO_2, CH_4 and SF_6 obtained from Tables 1, 5, 7 and 9 respectively in [21] are shown in terms of the corresponding temperatures $300 \le T \le 3273$ (K). Simulations have been performed for all these gases (gas properties including characteristic vibrational temperatures are shown in Table 1) close to the hydrodynamic limit at $\delta_0 = 100$, with $T_C = 300\,\mathrm{K}$ and $T_H = 3273\,\mathrm{K}$ ($T_0 = 1786.5\,\mathrm{K}$, $\beta = 10.91$). The rotational and vibrational collision numbers are $Z_{rot}^{(H)} = 5$ and $Z_{vib}^{(H)} = 50$. The Pr number is taken as a function of temperature according to the data in [21] (Tables 1, 5, 7, 9 in [21]). Once the problem is solved, an effective thermal conductivity $k_{eff}(y)$ is determined based on the Fourier law, which in the present dimensionless notation reads as

$$q_{tot} = \left[\frac{m}{2k_{\mathrm{B}}\delta_0\mu_0}\right] k_{eff}(y) \frac{\partial \tau_{tot}}{\partial y} \tag{30}$$

with the spatial derivative $\partial \tau_{tot}/\partial y$ being approximated by central differences. Previous studies (see [22,23] and references therein for monatomic gases and [24] for a diatomic gas), have shown that $k_{eff}(y)$ approximates extremely well the Chapman-Enskog value of the thermal conductivity in a central strip of the domain, provided its boundaries are sufficiently far from the walls where the Knudsen layers cause deviations from the hydrodynamic behavior. The computed $k_{eff}(y)$ is plotted in Fig. 2 and compared to the experimental one. As it is seen, the computational results are in excellent agreement with the experimental data in the whole region

between the plates, except very close to walls, where, as it is shown in Section 5.3, even at large values of δ_0, the Fourier constitutive law is not valid.

Based on all above the effectiveness of the Holway kinetic model to simulate this heat transfer configuration is demonstrated. Also, the efficiency of the implemented computational scheme and the accuracy of the deduced numerical results are verified.

5.2 Effect of vibrational degrees of freedom

The effect of θ_V on the heat fluxes and other macroscopic quantities is investigated. The analysis is for diatomic gases ($j=2$) with hard sphere (HS) molecules ($\omega=0.5$) in order not to name a specific gas and the concluding remarks to be as general as possible.

However, before we proceed it is interesting to examine the effect of the prescribed collision numbers $Z_{rot}^{(H)}$ and $Z_{vib}^{(H)}$ on the results. A computational sensitivity analysis related to these two parameters is shown in Tables 4 and 5. The temperature ratio of the two plates is taken large and equal to $\beta=5$, while the parameter $\theta_V=[0.1,5]$. Also, the results are for $\delta_0\times\mathrm{Pr}=71.4$ without being necessary to specify exactly either of the two quantities. However, since for a diatomic gas $\mathrm{Pr}\simeq 0.7$ the analysis is performed, in purpose, at high values of $\delta_0\simeq 10^2$, where the effect of the rotational and vibrational degrees of freedom is more dominant. Based on the above input data, in Table 4, all heat fluxes are tabulated by keeping the vibrational collision number constant, $Z_{vib}^{(H)}=50$, while the rotational one varies as $Z_{rot}^{(H)}\in[3,80]$. The corresponding results for constant rotational number $Z_{rot}^{(H)}=5$ and the vibrational number varying as $Z_{vib}^{(H)}\in\left[5,10^3\right]$ are tabulated in Table 5. As $Z_{rot}^{(H)}$ is increased, with $Z_{vib}^{(H)}$ being constant, q_{tr} is slightly increased not more than 2 % and q_{rot} is slightly decreased not more than 3 %. Also q_{vib} and q_{tot} are not affected at all for the significant figures shown. These observations are valid for both $\theta_V=0.1$ and 5. As $Z_{vib}^{(H)}$ is increased, with $Z_{rot}^{(H)}$ being constant, the variation in q_{tr} and q_{rot} is very small not exceeding 5 % for both θ_V. More interesting is the effect of $Z_{vib}^{(H)}$ on q_{vib}, which for $\theta_V=0.1$ is decreased only by 3%, while for $\theta_V=5$ is decreased by 36%. However, in this latter case the vibrational heat flux is one order of magnitude smaller than the translational one and

therefore, once again, there is no variation of the total heat flux q_{tot} with respect to the vibrational collision number. The fact that the total heat flux remains invariant in terms of $Z_{rot}^{(H)}$ and $Z_{vib}^{(H)}$ is of major importance and reduces the introduced modeling error, particularly when, comparisons with experimental work are performed. The effect of $Z_{rot}^{(H)}$ and $Z_{vib}^{(H)}$ on the density and temperatures distributions is negligible. Also, in general the effect of $Z_{rot}^{(H)}$ and $Z_{vib}^{(H)}$ is decreased as the temperature difference between the plates is decreased.

Next, in Table 6 the translational, rotational and vibrational heat fluxes as percentage of the total heat flux along with the total heat fluxes are provided for a diatomic HS gas ($j=2$, $\omega=0.5$) and for various values of θ_V and of the product $\delta_0 \times \mathrm{Pr}$ with $\beta=1.1$. The collision numbers are set to $Z_{rot}^{(H)}=5$ and $Z_{vib}^{(H)}=50$. The percentage results are at the hot plate ($y=-1/2$), while q_{tot} remains constant between the plates. Depending upon θ_V the ratios of the translational, rotational and vibrational heat fluxes over the total one vary as $0.5 \le q_{tr}/q_{tot} \le 0.66$, $0.23 \le q_{rot}/q_{tot} \le 0.32$ and $0.05 \le q_{vib}/q_{tot} \le 0.25$ respectively. As expected, independently of θ_V, the rotational heat flux is about 43-50% of the corresponding translational ones. Also, as θ_V is decreased the vibrational part becomes of the same order of the rotational one and corresponds to about 25% of the total heat flux. This is justified by the fact that, as the parameter θ_V is decreased the mean temperature is increased, thus causing activation of a larger number of vibrational degrees of freedom. It is noted that in the case of $\theta_V=0.1$ the vibrational degrees of freedom are almost fully excited with $\zeta_v \cong 1.9$. The corresponding mean values of ζ_v for $\theta_V=1$ and 5 is about 1.2 and 0.07 respectively. These results are valid in the whole range of the gas rarefaction examined. It is noted that the percentage of each part of heat flux to the total heat flux remains almost constant with regard to δ_0.

The dimensionless translational $e_{tr}\left(y\right)$, rotational $e_{rot}\left(y\right)$ and vibrational $e_{vib}\left(y\right)$ energies of a diatomic HS gas ($j=2$, $\omega=0.5$, $Z_{rot}^{(H)}=5$, $Z_{vib}^{(H)}=50$) are shown in Fig. 3 for various values of $\delta_0 \times \mathrm{Pr}$ with $\beta=1.1$ and $\theta_V=\left[0.1,5\right]$. The translational and vibrational energies are independent of θ_V, while the vibrational energy depends strongly on θ_V. Therefore the latter one

is presented in two subfigures. The vibrational energy for $\theta_V = 0.1$ is approximately 28 times higher than the corresponding one for $\theta_V = 5$, with the exact number depending on the position between the plates and on the gas rarefaction. The ratio of the vibrational distribution energies for $\theta_V = 0.1$ and $\theta_V = 5$ is increased moving from the hot towards the cold plate wall. Also, all energies are higher, as they should, near the hot wall than the corresponding ones at the cold wall.

In Fig. 4 the dimensionless vibrational temperature is plotted for the same input parameters as in Fig. 3. At large $\delta_0 \times \mathrm{Pr}$ the vibrational temperatures for $\theta_V = [0.1, 5]$ almost coincide, while as $\delta_0 \times \mathrm{Pr}$ (or δ_0) is decreased they depart of each other with $\tau_{vib}(y)$ for $\theta_V = 5$ being higher than the corresponding ones for $\theta_V = 1$. This latter behavior is probably not expected but it may be explained by considering the reported vibrational energies for $\theta_V = [0.1, 5]$ in Fig. 4 and that in diatomic gases $\tau_{vib} = \theta_V \Big/ \ln[1 + \frac{\theta_V}{e_{vib}}]$. Based on the above this behavior is contributed to the relative decrease of e_{vib} with regard to the increase of θ_V. It is also seen in the analytical expressions provided in the free molecular limit in Appendix B (Eq. B3). Furthermore, the parameter θ_V has no effect on the number density distribution and the corresponding plots are omitted. Since θ_V has a very small effect on the translational and rotational temperatures they are not plotted here and they may be found in [14]. In large values of δ_0 the vibrational temperature is thermally equilibrated with the translational and rotational temperatures ($\tau_{tr} \simeq \tau_{rot} \simeq \tau_{vib}$) independent of θ_V.

5.3 Heat fluxes for specific gases

In this subsection results are provided for the nonpolar polyatomic gases of N_2, O_2, CO_2, CH_4 and SF_6 based on the Holway kinetic model with temperature ratio $\beta = 1.1$ in a wide range of the rarefaction parameter δ_0. Two values of the reference mean temperature, namely $T_0 = 500\,\mathrm{K}$ and $2000\,\mathrm{K}$, are considered. . The typical values of $Z_{rot}^{(H)} = 5$ and $Z_{vib}^{(H)} = 50$ are used. The parameters of each gas are given in Table 1 and the Pr number is a function of temperature according to [21].

In Fig. 5 the rotational, vibrational and total heat fluxes at the hot wall ($y=-1/2$) are given in a wide range of the rarefaction parameter δ_0. It is seen that the rotational heat fluxes are in practice independent of the mean temperature T_0. The rotational heat fluxes q_{rot} of the linear gases (N_2, O_2, CO_2) are very close to each other (almost coincide) and the same happens for the nonlinear gases (CH_4, SF_6) with the latter ones being 30 - 60 % higher than the former ones for both T_0. The vibrational heat fluxes depend on T_0 and this dependency becomes stronger as, depending upon the working gas, the characteristic vibrational temperatures are decreased and consequently the number of vibrational degrees of freedom is increased. The vibrational heat fluxes of N_2 and O_2 are about the same with small dependency on T_0. However, for CO_2 there is a significant difference in q_{vib} as the mean temperature is increased from 500 K to 2000 K, which becomes even larger in the cases of CH_4 and SF_6. More specifically, since the SF_6 contains 15 vibrational modes and most of them are well excited at $T_0=500$ K is characterized compared to the other gases by the largest vibrational heat flux which is about 74 - 76 % of the total heat flux. On the other hand, since the one vibrational mode of N_2 is fully activated at 3371K, its vibrational heat flux is only about 2% and 19 % of the total heat flux when the mean temperature is $T_0=500$ K and 2000 K respectively. With regard to δ_0, it is noted that the previous remark, related to diatomic gases, i.e. that the percentage of each part of heat flux to the total heat flux remains almost constant in the whole range of gas rarefaction (see Table 6), is also valid for linear and nonlinear polyatomic gases.

Computations for SF_6 have been also performed with $T_0=300$ K and are shown in Fig. 6. The resulting vibrational heat flux corresponds up to 67% of the total heat flux. The remaining 33% is split between the translational and rotational heat fluxes with the latter one being about 75% of the former one.

In monatomic gases it has been shown that when the flow is in the hydrodynamic regime with non-continuum effects (large local gradients) the effective thermal conductivity concept may be successfully applied to compute the corresponding heat fluxes [22,23]. A similar investigation is performed here for polyatomic gases. Equation (30) is solved for the effective thermal conductivity $k_{eff}(y)$, which may be readily computed since all other quantities in Eq.

(30) are defined. In Fig. 7, indicative results of the variation of the $k_{eff}\left(y\right)$ over the corresponding experimental values in [21] is plotted along the distance between the plates. The working gas is N_2 ($\omega = 0.69$, $j = 2$) with $\delta_0 = 50$, $\beta = 1.1$, 4 and $\theta_V = 3.371$ ($T_0 = 1000\,\mathrm{K}$). It is noted that the computed effective and experimental thermal conductivities (also seen in Fig. 2) are not constant within the domain but they are both decreasing moving from the hot towards the cold plate along with the temperature. It is seen that in the region approximately defined by $-0.45 \le y \le 0.45$ the ratio is constant and equal to one, clearly indicating that under both weakly ($\beta = 1.1$) or highly ($\beta = 4$) non-equilibrium conditions the Fourier law works satisfactory far from the boundaries, i.e., outside the Knudsen layers. On the contrary, close to the boundaries, i.e., inside the Knudsen layers, the ratio departs from one, which is a clear indication that that in that regions the Fourier constitutive law is not valid. Also, the hot wall Knudsen layer is thicker than the corresponding one at the cold wall since the mean free path is an increasing function of temperature at constant pressure. Corresponding results are readily obtained for the other polyatomic gases. Thus, the effective thermal conductivity approximation may be also applied in polyatomic gases with excited vibrational degrees of freedom provided that the system Knudsen number is small.

6. Concluding remarks

The problem of heat transfer through rarefied polyatomic gases between parallel plates maintained at different temperatures has been considered by taking into consideration the gas rotational and vibrational degrees of freedom. The solution is obtained by the Holway kinetic model and the DSMC method. The very good agreement between the two approaches as well as with experimental data clearly demonstrates the capability of the Holway model to accurately simulate polyatomic gas heat transfer in the whole range of gas rarefaction for small, moderate and large temperature differences between the plates. As pointed out however, in Section 3, the Holway model for polyatomic gases inherits the same restrictions of the BGK model, being not recommended whenever both momentum and energy transport play an important role.

The translational, rotational, vibrational and total heat fluxes of N_2, O_2, CO_2, CH_4 and SF_6 are computed to examine the effect of the mean reference temperature and of the gas rarefaction with regard to the characteristic vibrational temperatures and the corresponding number of vibrational degrees of freedom of each gas. It has been shown that for gases with low and moderate characteristic excitation temperatures (e.g. CO_2, CH_4 and SF_6) the vibrational heat flux may be, even at ambient temperatures, a significant portion of the total heat flux independent of the gas rarefaction. For example in the case of SF_6 at reference temperatures of 300 K and 500 K the vibrational heat fluxes are 67% and 76% respectively of the corresponding total ones. The effective thermal conductivity approximation has been also studied finding out that it can be successfully applied in polyatomic gases to study non-equilibrium effects providing that the system Knudsen number is small.

Overall, the present work aims to provide some useful insight in the heat transfer design and optimization of technological applications operating in a temperature range where the vibrational modes of the involved gases are excited and must be taken into consideration. It is evident that in such heat transfer configurations modeling must include the effect of the vibrational degrees of freedom.

Acknowledgments

Part of the simulations have performed using the HELIOS supercomputer system at Computational Simulation Centre of International Fusion Energy Research Centre (IFERC-CSC), Aomori, Japan, under the Broader Approach collaboration between Euratom and Japan, implemented by Fusion for Energy and JAEA.

Appendix A: Relaxation rates in a homogenous gas

In order to achieve a proper comparison between the Holway kinetic model and the DSMC method, it is necessary to match the rotational and vibrational relaxation rates of the two approaches by accordingly relating $Z_{rot}^{(H)}$ with $Z_{rot}^{(DSMC)}$ and $Z_{vib}^{(H)}$ with $Z_{vib}^{(DSMC)}$. The corresponding analysis for the rotational relaxation rates has been done in [14].

Consider a spatially homogeneous diatomic gas at a constant equilibrium total temperature and an initial vibrational temperature which is different than the initial translational and rotational temperatures which are set equal to each other. Then, all partial temperatures will evolve and relax toward the constant equilibrium total temperature with a common rate determined by the collision frequency and vibrational relaxation numbers $Z_{rot}^{(i)}$ and $Z_{vib}^{(i)}$. By operating accordingly on the kinetic model equations the time evolution of the temperatures may be obtained. Then, the parameters $Z_{rot}^{(i)}$ and $Z_{vib}^{(i)}$ are accordingly fixed to ensure equivalent translational, rotational and vibrational relaxation rates in order to have a consistent comparison.

The kinetic model Eqs. (16) are rewritten for a time-dependent homogeneous system, i.e., by adding the time derivative term and omitting all space derivatives terms. Then, they are accordingly combined and the resulting equations are integrated over the velocity and energy spaces to yield the following relaxation kinetic equations:

$$\frac{dT_{tr}}{d\hat{t}} = \Pr \frac{\left(T_{tr}\right)^{1-\omega} P_0}{\left(T_0\right)^{1-\omega} \mu\left(T_0\right)} \left[\frac{1}{Z_{vib}^{(H)}} \left(T_{tot} - T_{tr}\right) + \frac{2}{5} \frac{1}{Z_{rot}^{(H)}} \left(T_{rot} - T_{tr}\right) \right] \tag{A1}$$

$$\frac{dT_{rot}}{d\hat{t}} = \Pr \frac{\left(T_{tr}\right)^{1-\omega} P_0}{\left(T_0\right)^{1-\omega} \mu\left(T_0\right)} \left[\frac{1}{Z_{vib}^{(H)}} \left(T_{tot} - T_{rot}\right) + \frac{3}{5} \frac{1}{Z_{rot}^{(H)}} \left(T_{tr} - T_{rot}\right) \right] \tag{A2}$$

$$\frac{d\left[T_{vib}\zeta_v\left(T_{vib}\right)\right]}{d\hat{t}} = \frac{\Pr}{Z_{vib}^{(H)}} \frac{\left(T_{tr}\right)^{1-\omega} P_0}{\left(T_0\right)^{1-\omega} \mu\left(T_0\right)} \left[T_{tot}\zeta_v\left(T_{tot}\right) - T_{vib}\zeta_v\left(T_{vib}\right) \right] \tag{A3}$$

All quantities are defined in Sections 2 and 3. The number density remains constant in time $\partial n / \partial \hat{t} = 0$. The relaxation rates of the kinetic model equations have been compared numerically with the corresponding ones of the DSMC method and it has been found that good agreement is observed by setting [34,14]

$$Z_i^{(H)} = \frac{\Pr}{30}\left(6-\frac{4}{\alpha}\right)\left(4-\frac{4}{\alpha}\right)Z_i^{(DSMC)}, \tag{A4}$$

where $i = rot, vib$ and $\alpha = 4/(2\omega - 1)$ is a parameter of the inverse power law potential which varies between the limits for Maxwell molecules ($\alpha = 4$) and hard sphere molecules ($\alpha \to \infty$).

Indicative results are demonstrated in Fig. 8, where the time evolution of the translational, rotational and vibrational temperatures toward the equilibrium temperature for a diatomic gas ($\Pr = 0.764$, $\omega = 0.74$, $P_0 = 0.1$ Pa, $\mu(T_0) = 94.55$ μPa s) [32] with initial temperatures $T_{tr}^{(i)}(0) = T_{rot}^{(i)}(0) = 3371\,\mathrm{K}$ and $T_{vib}^{(i)}(0) = 6742\,\mathrm{K}$, are shown. It is seen that for $Z_{vib}^{(DSMC)} = 50$ and $Z_{rot}^{(DSMC)} = 5$ there is very good agreement provided that using Eq. (A4), $Z_{vib}^{(H)} = 24.7$ and $Z_{rot}^{(H)} = 2.47$. Equation (A4) is used in Section 5.1 to define the rotational and vibrational collision numbers for the Holway kinetic model and the DSMC method in order to have a consistent comparison between the computed heat fluxes and the other macroscopic quantities.

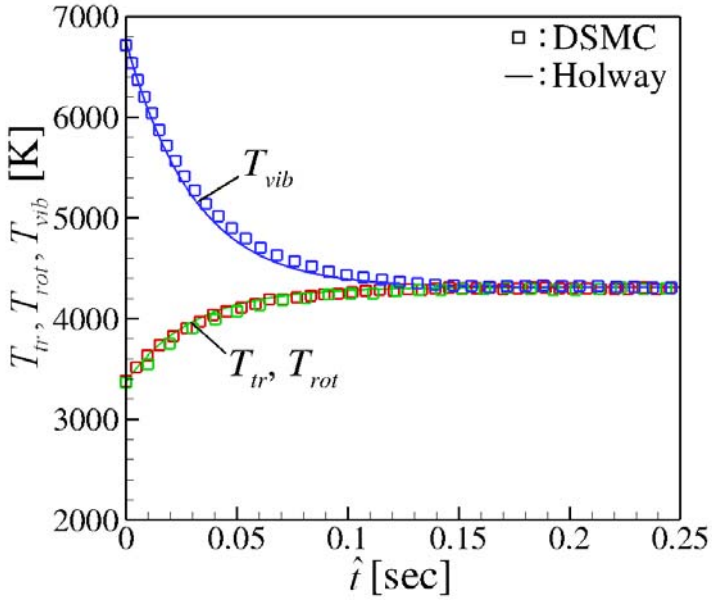

Figure 8: Translational-rotational-vibrational relaxation in a homogeneous gas.

Appendix B: Analytical solutions at the free molecular limit

In the free molecular limit ($\delta_0 = 0$) the right hand side of the kinetic model Eqs. (22) becomes zero and then, based on the associated boundary conditions closed form expressions for the reduced distributions functions $\boldsymbol{\Psi}$ are readily deduced. Next, they are substituted into the moment equations (24) to yield analytical results for the macroscopic distributions. It is noted that in the free molecular limit all moments remain constant at any position between the plates.

Following this procedure and using the boundary conditions (27) and (28) the translational and rotational heat fluxes in terms of the normalized temperature difference β are identical with those obtained in [14], while the vibrational heat flux is given by

$$q_{vib,fm} = \frac{1}{2\sqrt{\pi}} \frac{\sqrt{\tau_{w,C}\tau_{w,H}}}{\sqrt{\tau_{w,C}} + \sqrt{\tau_{w,H}}} \left[\tau_{w,H} \zeta_v \left(\tau_{w,H} \right) - \tau_{w,C} \zeta_v \left(\tau_{w,C} \right) \right] \tag{B1}$$

where $\tau_{w,H} = T_H / T_0 = 2\beta / (\beta + 1)$ and $\tau_{w,C} = T_C / T_0 = 2 / (\beta + 1)$, while ζ_v is the vibrational degrees of freedom as defined by Eqs. (25). The translational and rotational temperatures are obtained to be equal to each other and equal with $\tau_{tr,fm} = \tau_{rot,fm} = \sqrt{\tau_{w,C}\tau_{w,H}}$, while the vibrational temperature may also be deduced in an implicit form given by

$$\tau_{vib,fm} = \frac{\tau_{w,H}\sqrt{\tau_{w,C}}\zeta_v \left(\tau_{w,H} \right) + \tau_{w,C}\sqrt{\tau_{w,H}}\zeta_v \left(\tau_{w,C} \right)}{\zeta_v \left(\tau_{vib,fm} \right) \left(\sqrt{\tau_{w,C}} + \sqrt{\tau_{w,H}} \right)} . \tag{B2}$$

In the case of diatomic gases (B2) is simplified to deduce the explicit expression

$$\tau_{vib,fm,diatomic} = \frac{\theta_V}{\ln \left[1 + 2\theta_V \dfrac{\sqrt{\tau_{w,C}} + \sqrt{\tau_{w,H}}}{\tau_{w,H}\sqrt{\tau_{w,C}}\zeta_v \left(\tau_{w,H} \right) + \tau_{w,C}\sqrt{\tau_{w,H}}\zeta_v \left(\tau_{w,C} \right)} \right]} . \tag{B3}$$

Finally, the number density is $\rho_{fm} = 1$.

References

1. Y. G. Semyonov, S. F. Borisov, P. E. Suetin, Investigation of heat transfer in rarefied gases over a wide range of Knudsen number, International Journal of Heat and Mass Transfer, 27 (10), 1789-1799, 1984.
2. F. Sharipov, G. Bertoldo, Heat transfer through a rarefied gas confined between two coaxial cylinders with high radius ratio, Journal of Vacuum Science and Technology A 24 (6), 2087-2093, 2006.
3. S. Pantazis, D. Valougeorgis, Heat transfer between parallel plates via kinetic theory in the whole range of the Knudsen number, Paper 407, 5th European Thermal-Sciences Conference, 19-22/5/2008, Eindhoven, the Netherlands, 2008.
4. I. Graur, A. P. Polikarpov, Comparison of different kinetic models for the heat transfer problem, Heat Mass Transfer, 46 (2), 237-244, 2009.
5. S. Pantazis, D. Valougeorgis, Non-linear heat transfer through rarefied gases between coaxial cylindrical surfaces at different temperatures, European Journal of Mechanics B/Fluids, 29, 494-509, 2010.
6. H. Yamaguchi, K. Kanazawa, Y. Matsuda, T. Niimi, A. Polikarpov, I. Graur, Investigation on heat transfer between two coaxial cylinders for measurement of thermal accommodation coefficient, Physics of Fluids, 24, 062002, 2012.
7. S. K. Hsu, T. F. Morse, Kinetic theory of parallel heat transfer in a polyatomic gas, Physics of Fluids, 15 (4), 584-591, 1972.
8. P. Pazooki, S. K. Loyalka, Heat transfer in a polyatomic gas – I. Plane parallel plates, International Journal of Heat and Mass Transfer, 28 (11), 2019-2027, 1985.
9. S. J. O'shea, R. E. Collins, An experimental study of conduction heat transfer in rarefied polyatomic gases, International Journal of Heat and Mass Transfer, 35 (12), 3431-3440, 1992.
10. I. N. Larina, V. A. Rykov, Kinetic model of the Boltzmann equation for a diatomic gas with rotational degrees of freedom, Computational Mathematics and Mathematical Physics, 50, 2118-2130, 2010.
11. W. M. Trott, J. N. Castaneda, J. R. Torczynski, M. A. Gallis, D. J. Rader, An experimental assembly for precise measurement of thermal accommodation, Review of Scientific Instruments, 82, 035120, 2011.
12. C. Tantos, D. Valougeorgis, M. Pannuzzo, A. Frezzotti, G. L. Morini, Conductive heat transfer in a rarefied polyatomic gas confined between coaxial cylinders, International Journal of Heat Mass Transfer, 79, 378-389, 2014.
13. L. Wu, C. White, T. J. Scanlon, J. M. Reese, Y. Zhang, A kinetic model of the Boltzmann equation for non-vibrating polyatomic gases, Journal of Fluid Mechanics, 763, 24-50, 2015.
14. C. Tantos, D. Valougeorgis, A. Frezzotti, Conductive heat transfer in rarefied polyatomic gases confined between parallel plates via various kinetic models and the DSMC method, International Journal of Heat Mass Transfer, 88, 636-651, 2015.
15. P. Chevrier, M. Barrault, C. Fievet, J. Maftoul, J. Millon Fremillon, Industrial applications of high-, medium- and low-voltage arc modelling, J. Phys. D: Applied Physics, 30, 1346-1355, 1997.
16. M. Maiss, C. A. M. Brenninkmeijer, Atmospheric SF_6: Trends, Sources, and Prospects, Environmental Science and Technology, 32 (20), 3077-3086, 1998.

17. A. La Porte, R. E. Putman, The practical application of SF_6 and helium for condenser tube and air in leakage detection, Condenser Technology Conference, Conco Services Corporation, Boston, MA., August 1996.
18. S. Zhang, F. Yu, Piezoelectric Materials for High Temperature Sensors, Journal of the American Ceramic Society, 94, 3153–3170, 2011.
19. X. Jiang, K. Kim, S. Zhang, J. Johnson, G. Salazar, High-Temperature Piezoelectric Sensing, Sensors, 14, 144-169, 2014; doi:10.3390/s140100144.
20. I. Chakraborty, W. C. Tang, D. P. Bame, T. K. Tang, MEMS micro-valve for space applications, Sensors and Actuators A: Physical, 83, 188-193, 2000.
21. F. J. Uribe, E. A. Mason, J. Kestin, Thermal conductivity of nine polyatomic gases at low densities, Journal of Physical and Chemical Reference Data, 19 (5), 1123-1136, 1990.
22. M. A. Gallis, J. R. Torczynski, D. J. Rader, M. Tij, A. Santos, Normal solutions of the Boltzmann equation for highly nonequilibrium Fourier flow and Couette flow, Physics of Fluids, 18, 017104, 2006.
23. M. A. Gallis, J. R. Torczynski, Investigation of the ellipsoidal-statistical Bhatnagar–Gross–Krook kinetic model applied to gas-phase transport of heat and tangential momentum between parallel walls, Physics of Fluids, 23, 030601, 2011.
24. D. Bruno, A. Frezzotti, G. P. Ghiroldi, Oxygen transport properties estimation by classical trajectory- direct simulation Monte Carlo, Physics of Fluids, 27, 057101, 2015.
25. C. Shen, Rarefied Gas Dynamics: Fundamentals, Simulations and Micro Flows, Springer, 2005.
26. L. H. Holway, New statistical models for kinetic theory: Methods of construction, Physics of Fluids, 9 (9), 1658-1673, 1966.
27. J. C. Haas, V. S. Arpaci, G. S. Springer, Mass and heat transfer in a diatomic gas, J. Plasma Phys., 6, 547-560, 1971.
28. A. Frezzotti, A numerical investigation of the steady evaporation of a polyatomic gas, European Journal of Mechanics B/Fluids, 26, 93-104, 2007.
29. P. Andries, P. L. Tallec, J. P. Perlat, B. Perthame, The Gaussian-BGK model of Boltzmann equation with small Prandtl number, European Journal of Mechanics B/Fluids, 19, 813-830, 2000.
30. G. A. Bird, Molecular Gas Dynamics and the Direct Simulation of Gas Flows, Oxford University Press, Oxford, 1994.
31. C. Borgnakke, P. S. Larsen, Statistical collision model for Monte Carlo simulation of polyatomic gas mixture, Journal of Computational Physics, 18 (4), 405-420, 1975.
32. F. Bergemann, I. D. Boyd, New discrete vibrational energy model for the direct simulation Monte Carlo method, Progress in Astronautics and Aeronautics, 158, 174-183, 1994.
33. E. W. Lemmon, R. T Jacobsen, Viscosity and Thermal Conductivity Equations for Nitrogen, Oxygen, Argon, and Air, International Journal of Thermophysics, 25, 21-69, 2004.
34. B. L. Haas, D. B. Hash, G. A. Bird, F. E. Lumpkin, H. A. Hassan, Rates of thermal relaxation in direct simulation Monte Carlo methods, Physics of Fluids 6 (6), 2191-2201, 1994.

Table 1: Properties of working gases (in the 3rd column numbers in parenthesis indicate degeneracy).

Gas	Type of molecules	Characteristic vibrational temperature [K] Θ_V	Molecular weight [Kg] $m \times 10^{26}$	Viscosity [μPa s] μ_0	Viscosity index ω
N_2	linear ($j = 2$)	3371	4.65	61.40	0.69
O_2		2256	5.31	72.51	0.66
CO_2		960 (2)	7.31	62.01	0.7
		1930(1)			
		3390(1)			
CH_4	non-linear ($j = 3$)	1880 (3)	2.66	41.12	0.68
		2200 (2)			
		4200(1)			
		4350 (3)			
SF_6		520 (3)	24.3	59.82	0.69
		760 (3)			
		890 (3)			
		930 (2)			
		1120 (1)			
		1390 (3)			

Table 2: Dimensionless heat fluxes for N_2 ($j = 2$, $\mathrm{Pr} = 0.764$) with VHS molecules ($\omega = 0.74$) at the hot plate ($y = -1/2$) for various values of δ_0, $\beta = 5$ ($T_H = 5618$ K, $T_C = 1124$ K, $T_0 = 3371$K) and $\theta_V = 1$ ($Z_{rot}^{(DSMC)} = 5$, $Z_{vib}^{(DSMC)} = 50$, $Z_{rot}^{(H)} = 2.47$, $Z_{vib}^{(H)} = 24.7$).

δ_0	q_{tr}		q_{rot}		q_{vib}		q_{tot}	
	Holway	DSMC	Holway	DSMC	Holway	DSMC	Holway	DSMC
0	6.00E-01		3.00E-01		2.62E-01		1.16	
0.1	5.76E-01	5.76E-01	2.86E-01	2.83E-01	2.49E-01	2.47E-01	1.11	1.11
1	4.35E-01	4.41E-01	2.07E-01	2.01E-01	1.81E-01	1.72E-01	8.23E-01	8.14E-01
5	2.32E-01	2.43E-01	1.05E-01	1.02E-01	9.24E-02	8.45E-02	4.29E-01	4.30E-01
10	1.49E-01	1.58E-01	6.65E-02	6.53E-02	5.95E-02	5.42E-02	2.75E-01	2.77E-01
50	3.82E-02	4.05E-02	1.68E-02	1.65E-02	1.57E-02	1.43E-02	7.07E-02	7.13E-02
100	1.97E-02	2.08E-02	8.68E-03	8.35E-03	8.15E-03	7.48E-03	3.66E-02	3.66E-02

Table 3: Dimensionless heat fluxes for O_2 ($j = 2$, $\mathrm{Pr} = 0.751$) with VHS molecules ($\omega = 0.66$) at the hot plate ($y = -1/2$) for various values of δ_0, $\beta = 5$ ($T_H = 3760$ K, $T_C = 752$ K, $T_0 = 2256$) and $\theta_V = 1$ ($Z_{rot}^{(DSMC)} = 5$, $Z_{vib}^{(DSMC)} = 50$, $Z_{rot}^{(H)} = 2.62$, $Z_{vib}^{(H)} = 26.2$).

δ_0	q_{tr}		q_{rot}		q_{vib}		q_{tot}	
	Holway	DSMC	Holway	DSMC	Holway	DSMC	Holway	DSMC
0	6.00E-01		3.00E-01		2.62E-01		1.16	
0.1	5.76E-01	5.76E-01	2.86E-01	2.84E-01	2.50E-01	2.47E-01	1.11	1.11
1	4.38E-01	4.42E-01	2.09E-01	2.01E-01	1.82E-01	1.73E-01	8.29E-01	8.17E-01
5	2.35E-01	2.43E-01	1.06E-01	1.02E-01	9.33E-02	8.49E-02	4.34E-01	4.30E-01
10	1.51E-01	1.57E-01	6.73E-02	6.53E-02	6.01E-02	5.42E-02	2.78E-01	2.76E-01
50	3.87E-01	4.03E-01	1.70E-02	1.65E-02	1.59E-02	1.43E-02	7.16E-02	7.11E-02
100	2.00E-02	2.08E-02	8.80E-03	8.52E-03	8.25E-03	7.40E-03	3.71E-02	3.67E-02

Table 4: Effect of $Z_{rot}^{(H)}$ on the translational, rotational, vibrational and total heat fluxes at the hot plate ($y=-1/2$) for a diatomic HS gas ($j=2$, $\omega=0.5$) with $\beta=5$, $\delta_0\times\Pr=71.4$ and $Z_{vib}^{(H)}=50$.

$Z_{rot}^{(H)}$	q_{tr}		q_{rot}		q_{vib}		q_{tot}	
	$\theta_V=0.1$	$\theta_V=5$	$\theta_V=0.1$	$\theta_V=5$	$\theta_V=0.1$	$\theta_V=5$	$\theta_V=0.1$	$\theta_V=5$
3	2.13E-02	2.02E-02	9.35E-03	8.85E-03	9.02E-03	3.81E-03	3.97E-02	3.29E-02
5	2.14E-02	2.03E-02	9.29E-03	8.80E-03	9.02E-03	3.81E-03	3.97E-02	3.29E-02
7.5	2.14E-02	2.03E-02	9.25E-03	8.76E-03	9.02E-03	3.81E-03	3.97E-02	3.29E-02
10	2.15E-02	2.03E-02	9.22E-03	8.73E-03	9.02E-03	3.81E-03	3.97E-02	3.29E-02
20	2.15E-02	2.04E-02	9.15E-03	8.66E-03	9.02E-03	3.81E-03	3.97E-02	3.29E-02
40	2.16E-02	2.05E-02	9.10E-03	8.61E-03	9.02E-03	3.81E-03	3.97E-02	3.29E-02
60	2.16E-02	2.05E-02	9.08E-03	8.59E-03	9.02E-03	3.81E-03	3.97E-02	3.29E-02
80	2.16E-02	2.05E-02	9.07E-03	8.58E-03	9.02E-03	3.81E-03	3.97E-02	3.29E-02

Table 5: Effect of $Z_{vib}^{(H)}$ on the translational, rotational, vibrational and total heat fluxes at the hot plate ($y=-1/2$) for a diatomic HS gas ($j=2$, $\omega=0.5$) with $\beta=5$, $\delta_0\times\Pr=71.4$ and $Z_{rot}^{(H)}=5$.

$Z_{vib}^{(H)}$	q_{tr}		q_{rot}		q_{vib}		q_{tot}	
	$\theta_V=0.1$	$\theta_V=5$	$\theta_V=0.1$	$\theta_V=5$	$\theta_V=0.1$	$\theta_V=5$	$\theta_V=0.1$	$\theta_V=5$
5	2.12E-02	2.00E-02	9.30E-03	8.76E-03	9.21E-03	4.15E-03	3.97E-02	3.29E-02
10	2.13E-02	2.01E-02	9.28E-03	8.76E-03	9.15E-03	4.08E-03	3.97E-02	3.29E-02
25	2.13E-02	2.02E-02	9.28E-03	8.77E-03	9.07E-03	3.95E-03	3.97E-02	3.29E-02
70	2.14E-02	2.03E-02	9.30E-03	8.82E-03	9.00E-03	3.73E-03	3.97E-02	3.29E-02
100	2.14E-02	2.04E-02	9.30E-03	8.85E-03	8.97E-03	3.63E-03	3.97E-02	3.29E-02
400	2.15E-02	2.07E-02	9.32E-03	8.99E-03	8.91E-03	3.10E-03	3.97E-02	3.28E-02
700	2.15E-02	2.09E-02	9.32E-03	9.06E-03	8.89E-03	2.83E-03	3.97E-02	3.28E-02
1000	2.15E-02	2.10E-02	9.32E-03	9.10E-03	8.88E-03	2.66E-03	3.97E-02	3.27E-02

Table 6: Dimensionless total heat fluxes with the corresponding percentages of the vibrational, rotational and translational heat fluxes for a diatomic HS gas ($j = 2$, $\omega = 0.5$) at the hot plate ($y = -1/2$) with various values of $\delta_0 \times \mathrm{Pr}$, $\beta = 1.1$ and θ_V ($Z_{rot}^{(H)} = 5$, $Z_{vib}^{(H)} = 50$).

$\delta_0 \times \mathrm{Pr}$	$\theta_V = 5$				$\theta_V = 2$				$\theta_V = 1$				$\theta_V = 0.1$			
	tr	*rot*	*vib*	q_{tot}	*tr*	*rot*	*vib*	q_{tot}	*tr*	*rot*	*vib*	q_{tot}	*tr*	*rot*	*vib*	q_{tot}
0	63.1	31.5	5.39	8.51E-02	53.7	26.8	19.4	1.00E-01	51.0	25.5	23.5	1.05E-01	50.0	25.0	25.0	1.07E-01
7.14(-2)	63.2	31.4	5.36	8.08E-02	53.9	26.8	19.4	9.48E-02	51.2	25.4	23.3	9.98E-02	50.2	24.9	24.8	1.02E-01
7.14(-1)	64.2	30.5	5.22	5.91E-02	54.9	26.1	18.8	6.90E-02	52.2	24.8	22.9	7.26E-02	51.2	24.3	24.3	7.40E-02
3.57	65.8	29.2	5.01	2.93E-02	56.7	25.2	18.2	3.40E-02	54.0	24.0	22.0	3.57E-02	53.0	23.6	23.4	3.64E-02
7.14	66.1	28.9	4.99	1.83E-02	57.2	24.9	17.9	2.12E-02	54.5	23.8	21.6	2.22E-02	53.6	23.4	23.0	2.26E-02
35.7	66.1	28.6	5.26	4.58E-03	57.4	24.8	17.8	5.28E-03	54.8	23.9	21.3	5.53E-03	54.0	23.5	22.7	5.63E-03
71.4	65.9	28.6	5.37	2.37E-03	57.2	24.8	17.9	2.73E-03	54.7	23.8	21.4	2.85E-03	54.1	23.4	22.7	2.90E-03

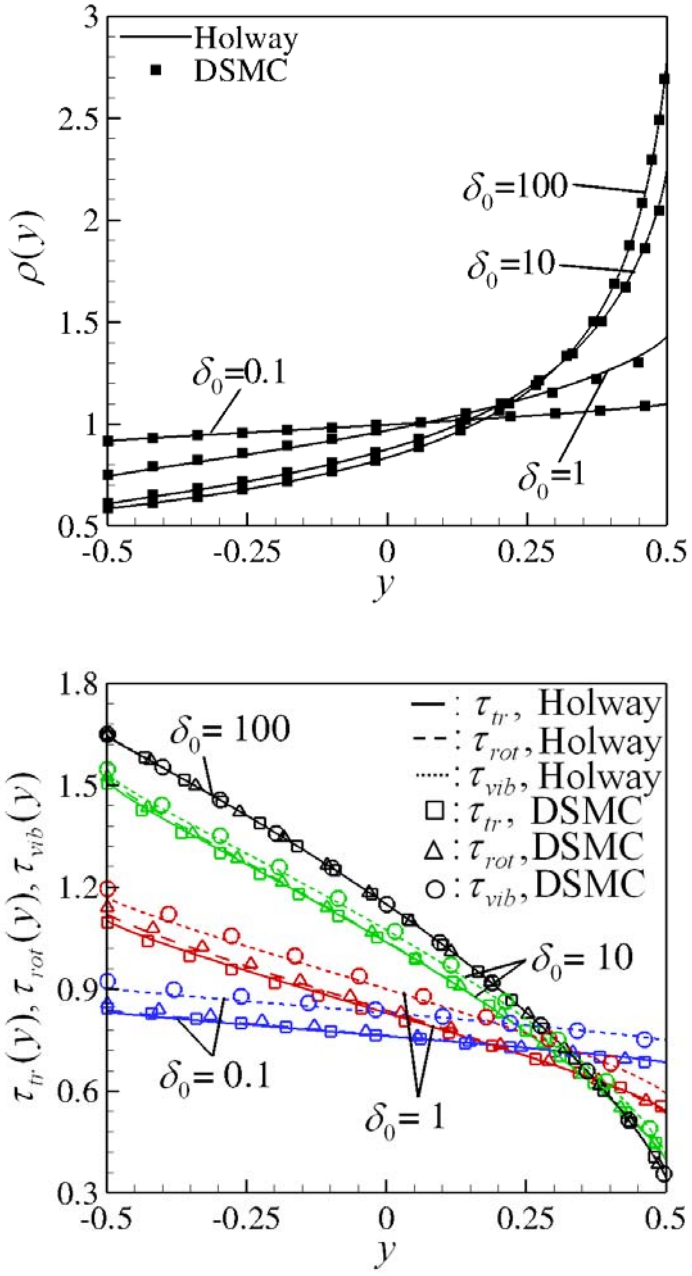

Figure 1: Comparison between the dimensionless density and temperature distributions of the Holway model and the DSMC method for N_2 ($j = 2$, $\Pr = 0.764$) with VHS molecules ($\omega = 0.74$) or various values of δ_0, $\beta = 5$ ($T_H = 5618\,\mathrm{K}$, $T_C = 1124\,\mathrm{K}$, $T_0 = 3371\mathrm{K}$) and $\theta_V = 1$ ($Z_{rot}^{(DSMC)} = 5$, $Z_{vib}^{(DSMC)} = 50$, $Z_{rot}^{(H)} = 2.47$, $Z_{vib}^{(H)} = 24.7$).

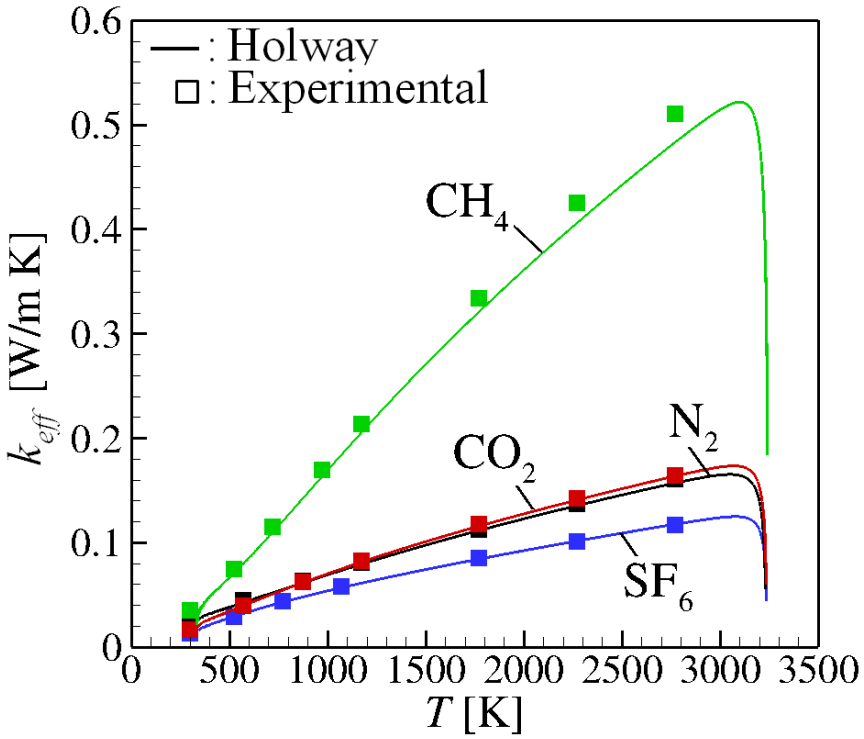

Figure 2: Comparison between the experimental thermal conductivities in [21] with $T_C = 300\,\mathrm{K}$, $T_H = 3273\,\mathrm{K}$ and the corresponding computed ones obtained by the Holway model with $\delta_0 = 100$ and $\beta = 10.9$ ($Z_{rot}^{(H)} = 5$, $Z_{vib}^{(H)} = 50$) for various gases.

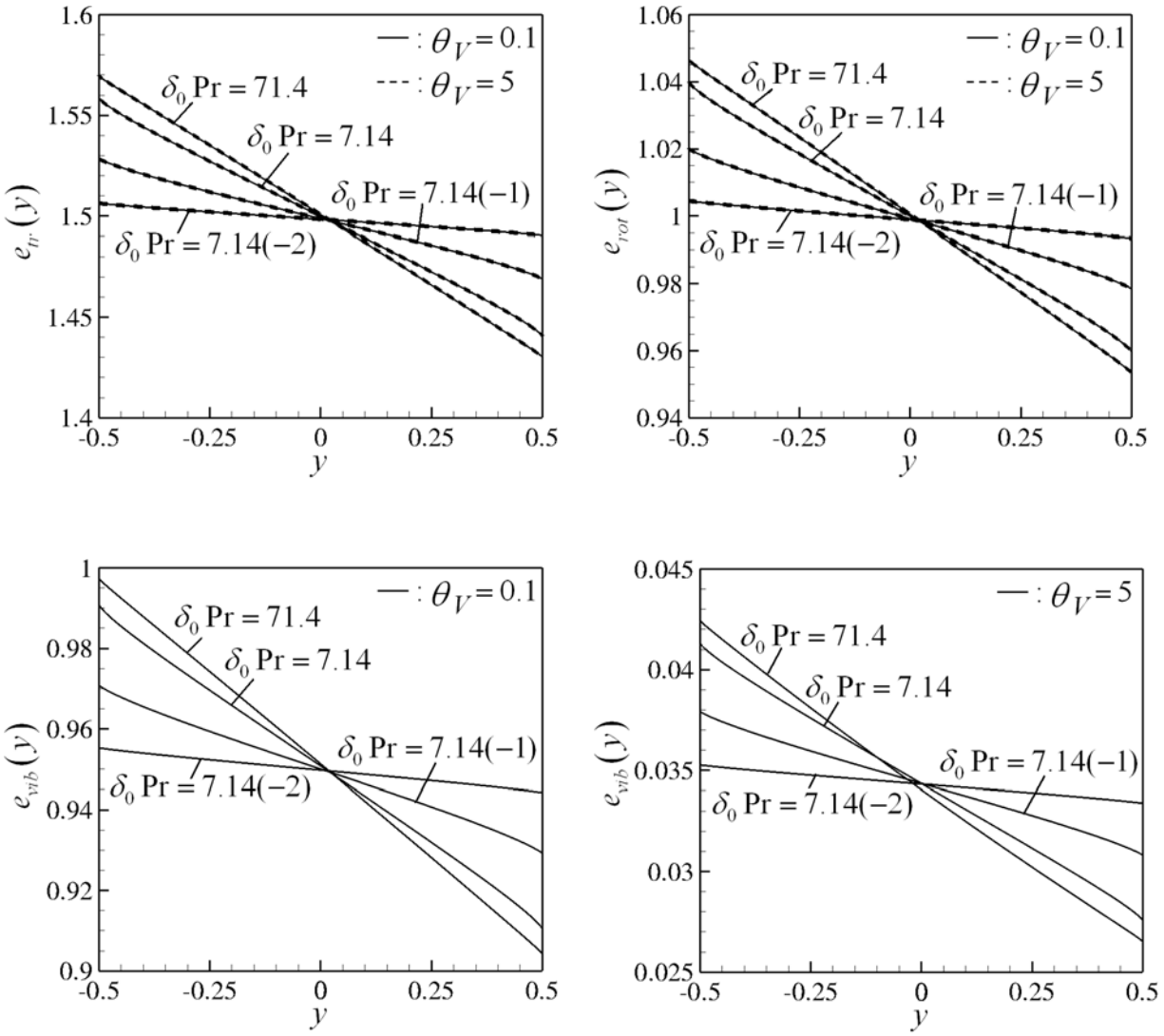

Figure 3: Dimensionless translational (left-up), rotational (right-up) and vibrational (down) energy distributions for a diatomic HS gas ($j = 2$, $\omega = 0.5$) with $\beta = 1.1$, various values of $\delta_0 \times \Pr$ and $\theta_V = [0.1, 5]$ ($Z_{rot}^{(H)} = 5$, $Z_{vib}^{(H)} = 50$).

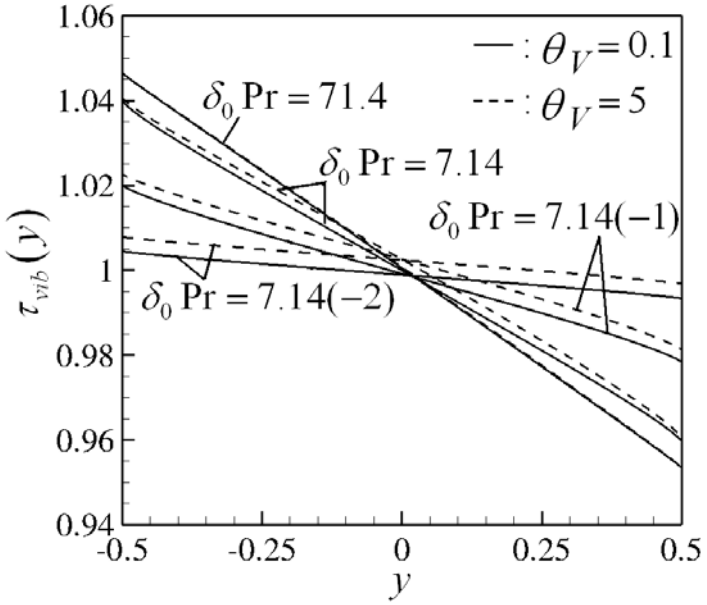

Figure 4: Dimensionless vibrational temperature distributions for a diatomic HS gas ($j = 2$, $\omega = 0.5$) with $\beta = 1.1$, various values of $\delta_0 \times \Pr$ and $\theta_V = [0.1, 5]$ ($Z_{rot}^{(H)} = 5$, $Z_{vib}^{(H)} = 50$).

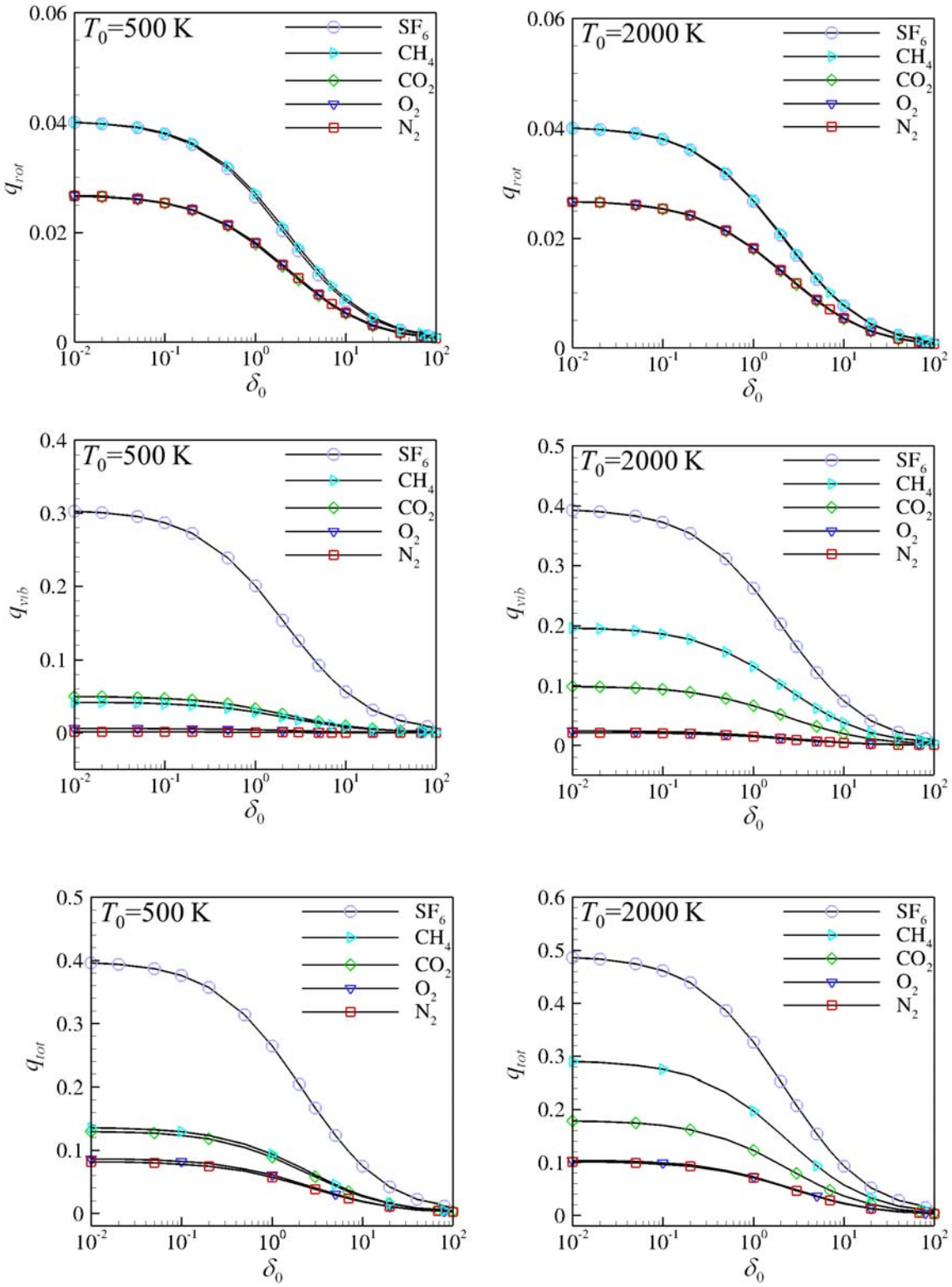

Figure 5: Dimensionless rotational (up), vibrational (middle) and total (down) heat fluxes at the hot plate ($y=-1/2$) in terms of δ_0 for various polyatomic gases, with $\beta=1.1$ and $T_0=500\,\mathrm{K}$ (left) and $T_0=2000\,\mathrm{K}$ (right) ($Z_{rot}^{(H)}=5$, $Z_{vib}^{(H)}=50$).

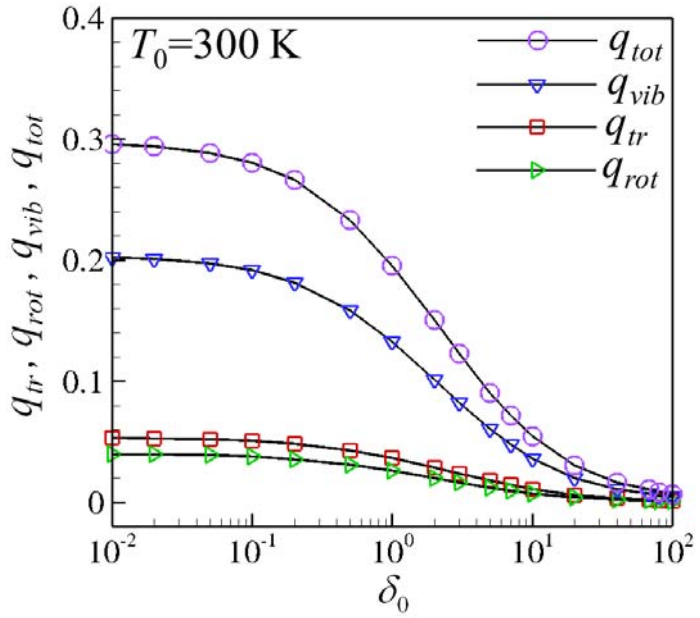

Figure 6: Dimensionless translational, rotational, vibrational and total heat fluxes at the hot plate ($y=-1/2$) in terms of δ_0 for SF_6, with $\beta=1.1$ and $T_0=300\,\mathrm{K}$ ($Z_{rot}^{(H)}=5$, $Z_{vib}^{(H)}=50$).

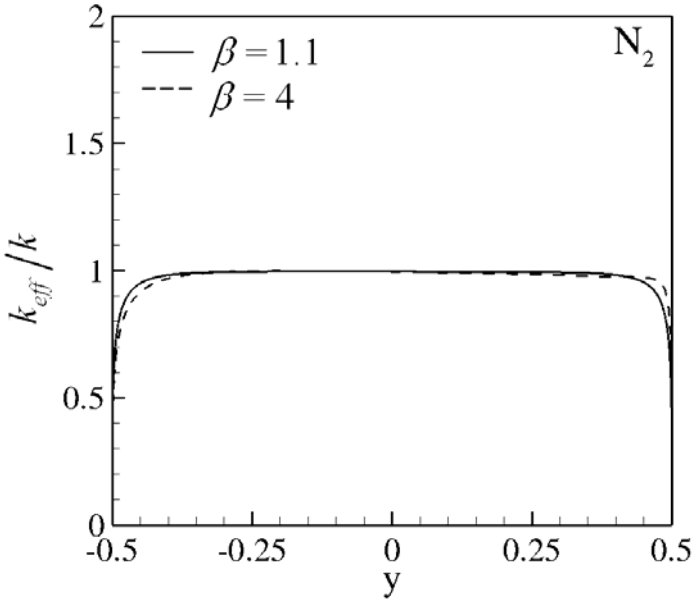

Figure 7: Ratio k_{eff}/k between the plates for N_2 ($\omega=0.69$, $j=2$) at $\delta_0=50$, $\beta=1.1$, 4 and $\theta_V=3.371\,\mathrm{K}$ ($Z_{rot}^{(H)}=5, Z_{vib}^{(H)}=50$).